ACS Sustainable Chemistry & Engineering

pubs.acs.org/journal/ascecg

Research Article

Synthesis of Silver Nanoparticle-Immobilized Antibacterial Anion-Exchange Membranes for Salinity Gradient Energy Production by Reverse Electrodialysis

Published as part of ACS Sustainable Chemistry & Engineering virtual special issue "Sustainable Energy and CO2 Conversion—Angel Irabien Festschrift".

Mine Eti, Aydın Cihanoğlu, Kadriye Özlem Hamaloğlu, Esra Altıok, Enver Güler,* Ali Tuncel, and Nalan Kabay*

Cite This: *ACS Sustainable Chem. Eng.* 2024, 12, 3977−3986

Read Online

ACCESS | Metrics & More | Article Recommendations

ABSTRACT: Biofouling, stemming from the attachment of living microorganisms, such as bacteria, which form resilient biofilms on membrane surfaces, presents a significant challenge that hampers the efficiency of anion-exchange membranes (AEMs) in reverse electrodialysis (RED) applications. This limitation curtails the generation of electrical power from salinity gradients, which notably is a sustainable form of energy known as osmotic energy. RED stands as a clean and promising process to harness this renewable energy source. This study aimed to impart antibacterial activity to synthesized AEMs by using silver nanoparticles (AgNPs). For that purpose, AgNPs were synthesized at 30 °C using two different pH values (6.0 and 9.0) and immobilized into synthesized AEMs using the dip-coating technique. In nanoparticle synthesis, ascorbic acid and trisodium citrate were used as a reductant and a stabilizer, respectively, to take control of the particle size and agglomeration behavior. The results indicated that AgNPs synthesized at pH 6.0 were dispersed on the AEM surface without agglomeration. The stability of AgNPs immobilized on the membrane surface was tested under low- and high-saline solutions. The antibacterial activities of AEMs were determined with the colony-counting method using Gram-negative (*Escherichia coli*) bacterial suspension. The viability of bacteria dramatically decreased after the immobilization of AgNPs in the AEMs. In the short- and long-term RED tests, it has been observed that the AEMs having AgNPs have high energy-generating potentials, and power density up to 0.372 W/m^2 can be obtained.

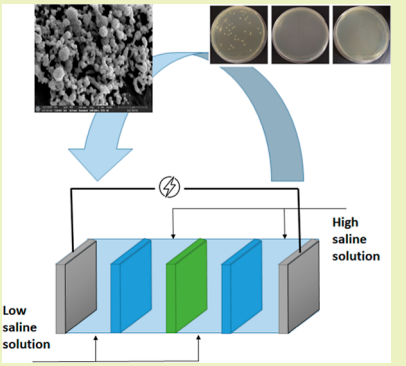

KEYWORDS: *biofouling, anion-exchange membranes, reverse electrodialysis, silver nanoparticles, antibacterial activity*

1. INTRODUCTION

Fouling of ion-exchange membranes (IEMs) is one of the most important constraints of the reverse electrodialysis (RED) process.[1] The source and type of feed solution have a significant impact on membrane fouling because of the wide range of pollutants present in different feed solutions. Colloidal (clays and flocs), organic (oils, polyelectrolytes, humic acid, and fulvic acid), scaling (mineral), and biological (bacteria and fungi) are the most prevalent forms of pollutants for membranes. Cation-exchange membranes (CEMs) in the RED system are more prone to scaling because of their structural and electrochemical characteristics, while anion-exchange membranes (AEMs) have less resistance to organic and biological fouling.[2] It is reported in the literature that energy harvesting performance by the RED system was dramatically decreased due to the presence of biological and organic fouling in the feedwater.[3−5] Even though pretreatment of feedwater is an alternative for eliminating foulants, imparting antifouling behavior to IEMs is an inevitable fact. It is possible to construct highly selective AEMs without increasing the membrane's electroresistance to prevent fouling. Various surface modification techniques can be used for this purpose. These modifications can be categorized as solution casting,[6] graft polymerization,[7] dip coating/immersion,[8] electrodeposition,[9] layer-by-layer deposition,[10,11] and plasma treatments.[12] Of the modification techniques listed, dip coating/immersion is the most suitable for surface coating because it is simple, low cost, additional chemical free, and highly repeatable.

Received: September 30, 2023
Revised: February 9, 2024
Accepted: February 9, 2024
Published: March 1, 2024

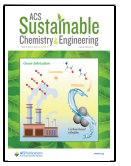

Silver is the most effective nanoparticle against viruses, bacteria, and other eukaryotic organisms due to their small size, high surface area, and ability to bind to matrices.[13,14] In addition to its antibacterial capabilities, covering AEMs with silver nanoparticles (AgNPs) improved its selective and ionic permeability,[15] ionic conductivity,[13] thermal stability,[16] and values compared to the unmodified membrane. In the study of Vaselbehagh et al., they looked at AEMs biofouling during RED tests and tried to modify their surfaces to make them less susceptible to biofouling.[17] Radzig et al. reported on the antibacterial action of AgNPs on Gram-negative bacteria along with the mechanism of action and the influence on the growth and biofilm formation.[18]

Nanocomposite AEMs for RED applications have not yet been prepared specifically yet. A restricted number of nanoparticles and polymeric materials have been employed to prepare IEMs specific to the RED system. In the majority of the RED research, commercial AEMs were utilized. Some studies were performed by coating their surface with a polyelectrolyte solution to create an antifouling membrane for RED systems, decreasing the membranes' ionic resistance, and increasing their selective permeability.[17,19,20] In this work, for the first time, antibacterial AgNP-immobilized AEMs were synthesized for salinity gradient energy production by RED, and their characterizations were done.

2. MATERIALS AND METHODS

The AEMs were prepared from a polymer solution by the casting method, followed by solvent evaporation. For the synthesis of membranes, poly(epichlorohydrin), PECH (37 wt % chlorine, Osaka Soda Co., Ltd.), as the active polymer, and poly(acrylonitrile), PAN (Mitsubishi Chemical Co. Ltd.), as the inert polymer were used. To provide good mechanical stability to the membranes, the cross-linker, 1,4-diazabicyclo[2.2.2]octane, DABCO (Reagent Plus ≥99%, Sigma-Aldrich), with diamine functionality was used. For the synthesis of AgNPs, silver nitrate ($AgNO_3$), ascorbic acid (AA) ($C_6H_8O_6$), trisodium citrate (TSC) ($Na_3C_6H_5O_7$), citric acid ($H_3C_6H_5O_7$), and sodium hydroxide ($C_6H_8O_6$) obtained from Sigma-Aldrich Co. were employed. The membrane synthesis details were given previously.[21] The membranes used in the study and their properties are given in Table 1.

Table 1. Properties of the Membranes[a]

membranes	ER-BR	SD (%)	IEC (mmol/g dry membrane)	FCD (mmol/g H_2O)
ER4-BR1.07	4−1.07	66.28	3.47	5.24
ER2-BR0.6	2−0.6	25.56	1.47	5.70

[a]ER: excess diamine ratio, BR: blend ratio, SD: swelling degree, IEC: ion-exchange capacity, FCD: fixed charge density. SD, IEC, and FCD calculations were given previously.[21]

2.1. Synthesis of AgNPs. AgNPs were synthesized in a water bath at a constant temperature of 30 °C using AA as a reductant and TSC as a stabilizer with solution pH values of 6.0 and 9.0. 8.0 mL of aqueous solution containing AA (6.0×10^{-4} M) and TSC (3.0×10^{-3} M) was adjusted to different pH values (6.0 and 9.0) by addition of 0.2 M citric acid or 0.1 M NaOH solution. 0.08 mL of 0.1 M $AgNO_3$ solution was added under a stirring speed of 900 rpm at 30 °C in a water bath. After 15 min, no further change in color (blue) took place, indicating that the reaction was completed.[22]

2.2. AgNP-Immobilized AEMs. Immobilization of the synthesized AgNPs to the AEMs was carried out in an acidic environment to observe the behavior of the membranes in an acidic environment. To this end, two different routes were followed. In the first way, the pH of the AgNP solution was adjusted to an acidic environment (pH 2.0), and then the membranes were added to this environment. In the second way, first, the membranes were added to the AgNP solution, and then the pH of the nanoparticle solution in which the membranes were submerged was adjusted to 2.0. The relevant membrane sample names and conditions are given in Table 2. The AgNP solution immobilization time was adjusted to 24 h.

Table 2. Immobilization of the Synthesized AgNPs to AEMs

samples	conditions
ER4-BR1.07	diamine ratio: 4; blend ratio: 1.07
1 (pH 6.0)	ER4-BR1.07 membranes were washed with distilled water for 24 h and then immersed in AgNP solution
2 (pH 9.0)	
3 (pH 6.0−1)[a]	the pH of the AgNP solution was adjusted to pH 2.0 first with the help of H_2SO_4, and then the washed membranes were added to the medium
4 (pH 9.0−1)[a]	
5 (pH 6.0−2)[b]	the washed membranes were immersed in the AgNP solution first, and then the pH of the medium was adjusted to 2.0 with the help of H_2SO_4
6 (pH 9.0−2)[b]	

[a]Represents the first way. [b]Represents the second way.

2.3. Stability Studies. The stability of AgNPs on the membrane surface was checked under two different saline water conditions. To this end, the AgNP-immobilized AEMs were exposed to 0.017 and 0.5 M NaCl solutions for 1 and 6 h, respectively. An inductively coupled plasma mass spectrometer (PerkinElmer DRC II model ICP−MS) was used for the measurement of silver ions released during the stability tests. The AgNP-attached membranes (5 mg) were dissolved in HNO_3. Then, centrifugation (5000 rpm for 5 min) was made to remove membranes that could not be dissolved. Subsequently, 1 mL of sample was taken from the supernatant, and ICP−MS analysis was made. Thus, the values obtained from ICP−MS analysis indicated the silver content of the membranes. With the calculations made from these values, the percentages of silver released from the membranes in the stability tests were calculated.

2.4. Characterizations. The particle sizes of AgNPs were measured with a Malvern Zeta sizer device. The UV−vis absorption spectra were obtained with a Thermo Scientific Genesys 20 UV−vis spectrophotometer. The chemical structure of the membranes was determined by Fourier transform infrared (FTIR) spectroscopy (PerkinElmer Spektrum 100) analysis. Thermo Scientific Apreo S model scanning electron microscopy (SEM), energy dispersive X-ray (EDX) mapping, and Thermo Scientific K-Alpha model X-ray photoelectron spectroscopy (XPS) were utilized for structure analyses of the membranes, determining the particle loading amount and homogeneity on the membrane surface. Ion-exchange capacity, swelling degree, and fixed charge density analysis details were calculated as reported before.[21]

2.5. Antibacterial Activity of AEMs. The antibacterial activities of the bare and AgNP-immobilized AEMs were determined using the model Gram-negative bacterial (*Escherichia coli*) suspension with the colony counting method according to the ASTM E2149 standard protocol. First, *E. coli* was inoculated in Mueller−Hinton agar. Then, the bacteria were incubated at 37 °C. After incubation, bacterial colonies were picked off with a swab and mixed with 0.1% (w) peptone water to adjust the concentration to the value of 0.5 McFarland (2.5×10^7 CFU/mL) standard scale. Next, the bacterial suspension was diluted with the nutrient broth (the dilution ratio is 1:9 bacterial suspension/nutrient broth) to adjust the concentration to 2.5×10^6 CFU/mL, and this was used as a stock suspension for the antibacterial tests. Before the antibacterial tests, membrane coupons (effective size: 3 cm × 3 cm) were first sterilized using UV light for 30 min (each side was exposed to UV light for 15 min). Then, 100 μL of the stock bacterial suspension was added into a 250 mL Erlenmeyer flask containing 50 mL of phosphate-buffered saline solution.

https://doi.org/10.1021/acssuschemeng.3c06320
ACS Sustainable Chem. Eng. 2024, 12, 3977−3986

Next, the membrane coupons were immersed in the bacterial suspension in the Erlenmeyer flask and shaken at 200 rpm for 24 h at 37 °C. Finally, the bacterial suspension was spread on the LB (Luria−Bertani) broth plates with 10^{-2} and 10^{-4} dilution rates and incubated for 24 h at 37 °C, and the colonies were counted. In antibacterial activity calculation, the inoculum solution (without containing any membrane) was used as a control. The antibacterial activity test was repeated three times (n = 3). The bactericidal rate was calculated using eq 1.[23]

$$\text{Antibacterial rate, \%}\left(\frac{\text{CFU}}{\text{mL}}\right) = \frac{N_P - N_M}{N_P} \times 100 \quad (1)$$

where N_P and N_M are the number of visual bacteria colonies on the agar plate after contacting with the bare and AgNP-modified membranes, respectively.

2.6. RED Studies. In the RED studies, unmodified PECH-C membranes (ER2-BR0.6) and AgNP-immobilized PECH-C membranes (ER2-BR0.6) were used as AEMs together with NEOSEPTA CMX membranes used as CEMs. The properties of NEOSEPTA CMX are given in Table 3. Operating conditions of the RED test are summarized in Table 4.

Table 3. Properties of the NEOSEPTA CMX Membranes

ion-exchange capacity (mmol/g)	1.64 ± 0.01
area resistance (Ω cm^2)	3.43 ± 0.16
permselectivity (%)	92.5 ± 0.6
swelling degree (%)	21.5 ± 0.2
thickness (μm)	181 ± 2.0

Table 4. Operating Conditions of the RED Test

flow rates of feed solutions (mL/min)	30, 75, 120
flow rate of the electrode solution (mL/min)	300
concentration of the feed solutions (g/L)	dilute NaCl solution: 1
	concentrated NaCl solution: 30
electrode solution	0.25 M NaCl
	0.05 M $K_3Fe(CN)_6$
	0.05 M $K_4Fe(CN)_6$
AEMs and CEMs	ER2-BR0.6 and NEOSEPTA CMX
salt ratio (g NaCl/L less-saline solution/g NaCl/L high-saline solution)	1:30
number of membrane pairs	3

3. RESULTS AND DISCUSSION

3.1. Characterization of AgNPs and Immobilized AEMs. The particle size distributions of the AgNPs synthesized at pH 6.0 and 9.0 are given in Figure 1. The average particle size of AgNPs at pH 6.0 was 107.4 nm and that at pH 9.0 was 96.92 nm. Qin et al. determined the AgNPs produced at pH 6.0 and pH 9.0 as 89 and 62 nm, respectively,[22] while Steinigeweg and Schlücker determined the sizes of hemispherical as 83.9 nm ± 26.2%.[24] The sizes of the AgNPs synthesized in this study are consistent with the results given in the literature.

The UV−vis absorption spectra of AgNPs prepared at pH 6.0 and 9.0 are given in Figure 2. The wavelengths related to the maximum absorbance were measured as 432 and 442 nm for AgNPs prepared at pH 9.0 and pH 6.0, respectively. Qin et al. obtained the wavelengths of AgNPs produced at pH 6.0 and pH 9.0 as 480 and 433 nm, respectively. In the other studies, the wavelength of AgNPs was found as in the range of 402−462 nm.[25−28] In the literature, it was reported that sodium

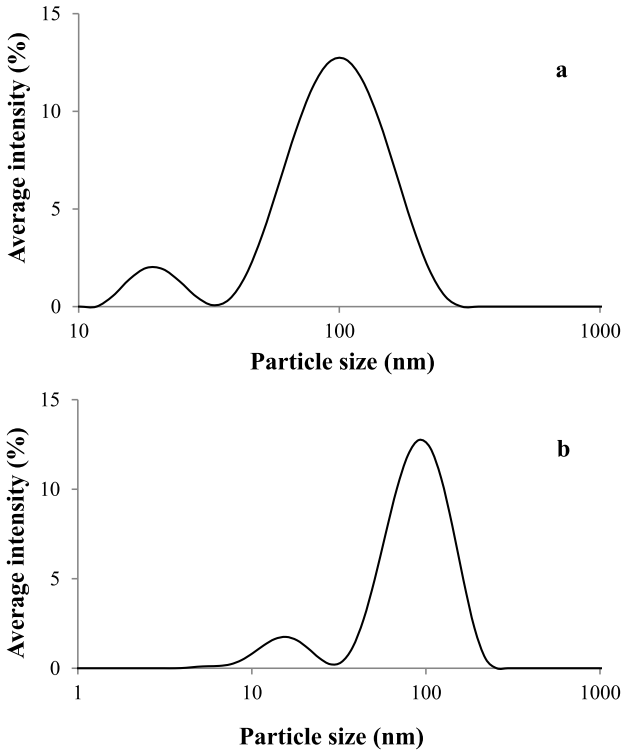

Figure 1. Size distribution of AgNPs produced at (a) pH 6.0 and (b) pH 9.0.

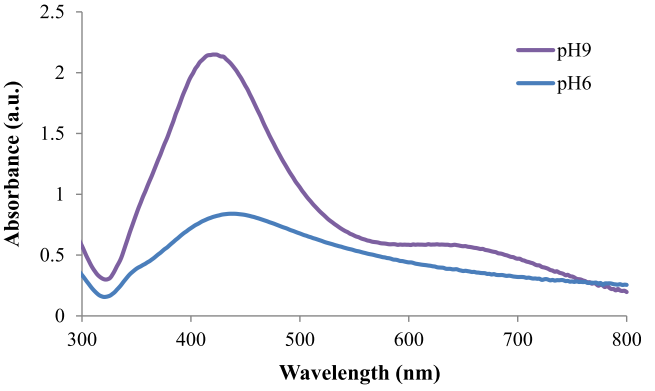

Figure 2. UV−vis spectra of AgNPs prepared at pH 6.0 and pH 9.0.

borohydride was used as a primary reductant and TSC as a secondary reductant as well as a stabilizing agent.

It was predicted that the negatively charged AgNPs would be better immobilized to the membranes by the electrostatic interaction of the membranes with protonated amine groups in an acidic environment. The FTIR analysis was performed to understand whether there is degradation in the membrane structure in an acidic environment. The analysis results showed that no change was observed in the wavenumbers showing −C≡N and C−N bonds in the FTIR spectra of membranes immersed in an acidic environment (pH 2) (Figure 3). Since no degradation was observed in the membranes in an acidic environment, AgNPs were produced, and immobilization on the membranes in an acidic environment was carried out by a dipping method.

The SEM images of the AEMs after nanoparticle immobilization are given in Figures 4 and 5. It is observed that there is an agglomeration in membranes after immobiliza-

https://doi.org/10.1021/acssuschemeng.3c06320
ACS Sustainable Chem. Eng. 2024, 12, 3977−3986

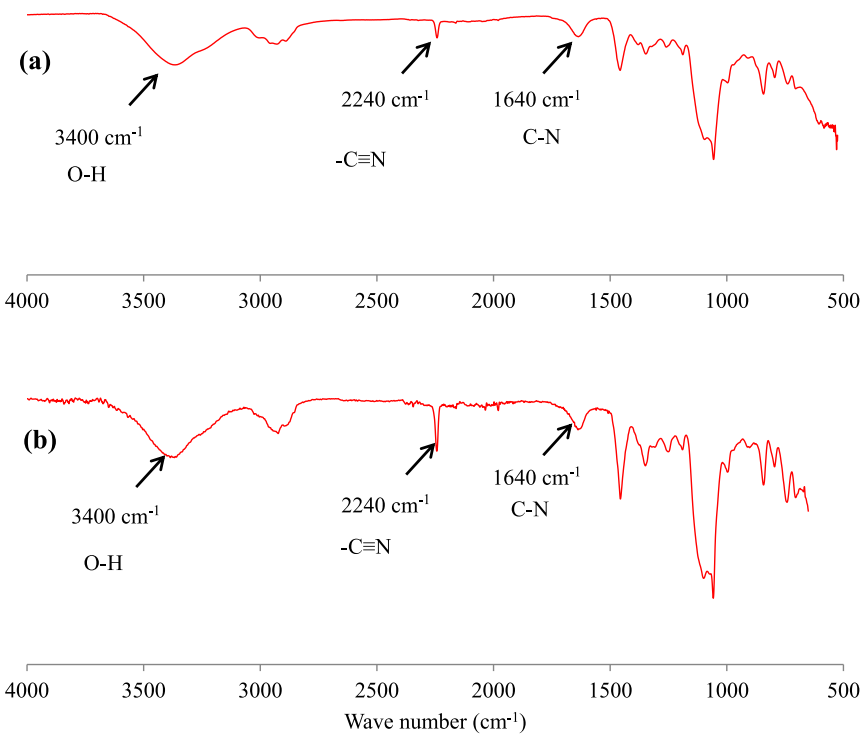

Figure 3. FTIR results of membranes immersed in (a) acidic and (b) neutral environments.

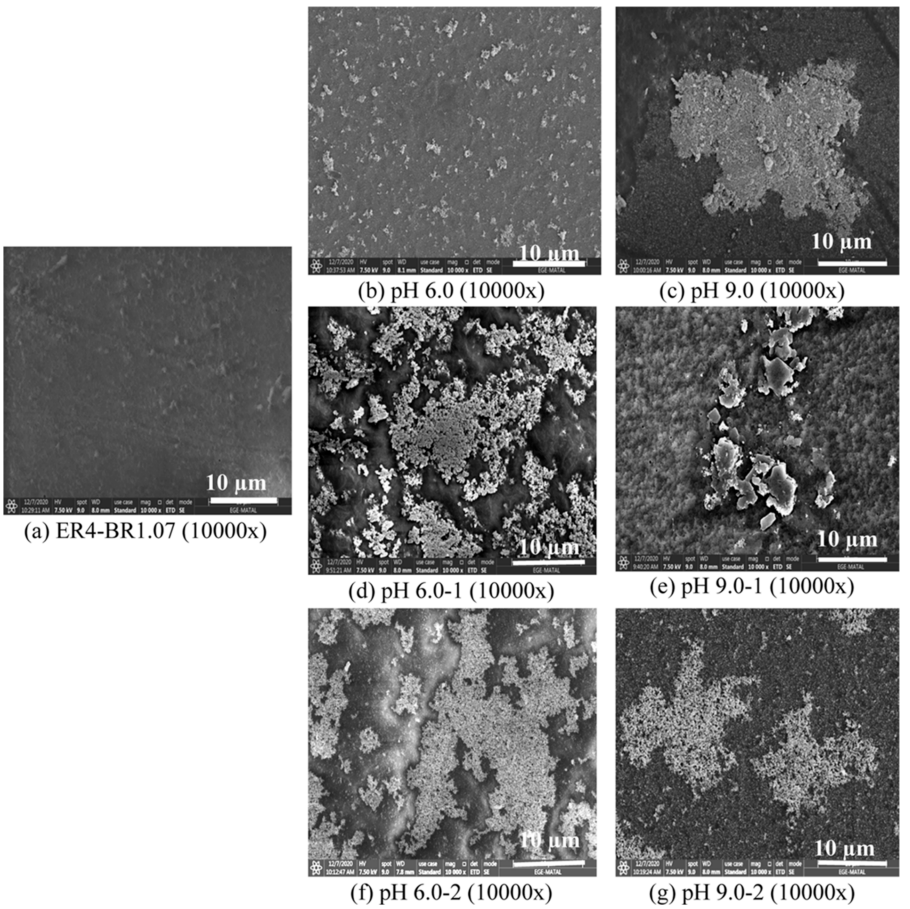

Figure 4. SEM surface images after nanoparticle immobilization to membranes (10,000×).

https://doi.org/10.1021/acssuschemeng.3c06320
ACS Sustainable Chem. Eng. 2024, 12, 3977−3986

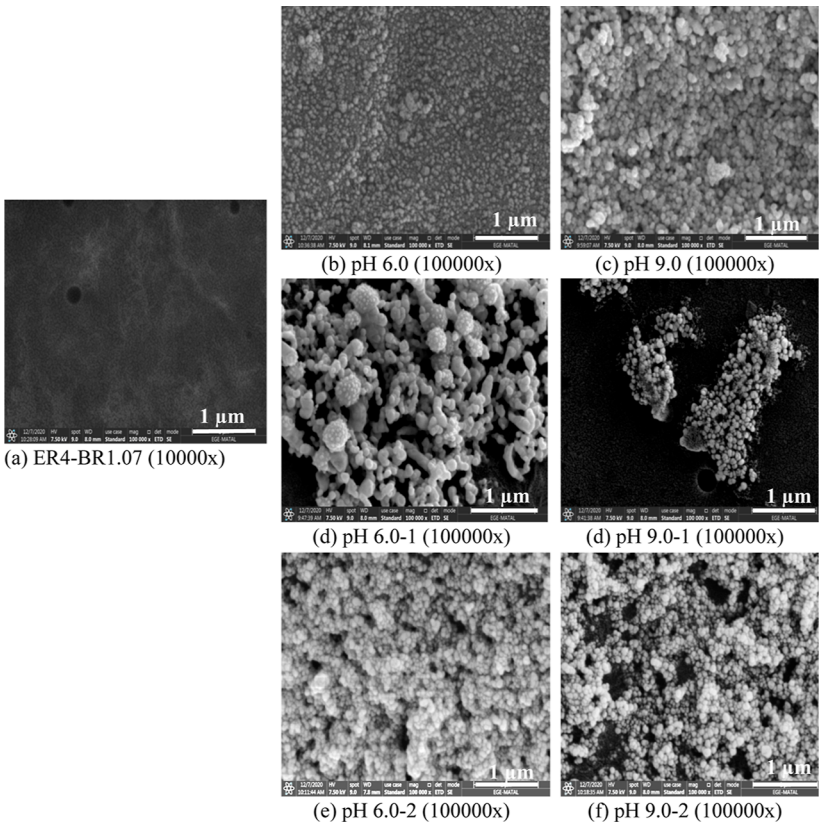

Figure 5. SEM surface images after nanoparticle immobilization to membranes (100,000×).

tion of AgNPs produced at pH 9.0. At high pH values, the rate of chemical reduction is high, and this caused the nanoparticles to aggregate. It is observed that the particle distribution is homogeneous after the immobilization of the AgNPs produced at pH 6.0 to the membrane without interacting with the acidic medium (pH 2.0; Figures 4b and 5b). Agglomerations were formed in pH 9.0 medium (Figures 4c and 5c). When AA is used as a reducing agent, the reduction reaction occurs slowly at high pH and causes AgNPs to agglomerate and grow on the membrane surface. It was observed that the best dispersion was observed in membranes prepared at pH 6.0.

The overall XPS spectrum for chemical component determination on the surface of AgNP-immobilized membranes (ER4-BR1.07) is given in Figure 6. It can be seen that all the elements (O, Ag, N, C, and Cl) expected to be on the membrane surface are detected. The O, C, N, and Cl elements are from the structure of the PECH-based AEM, and Ag is observed because of the AgNPs immobilized on the membrane surface.

When the Ag 3d core-level XPS spectrum given in Figure 7 is examined, specific Ag 3d bands belonging to metallic Ag can be seen at 368.4 and 374.4 eV. In addition, the absence of a specific 369.4 eV band belonging to Ag nanoclusters indicates that AgNPs are homogeneously immobilized on the membrane surface.

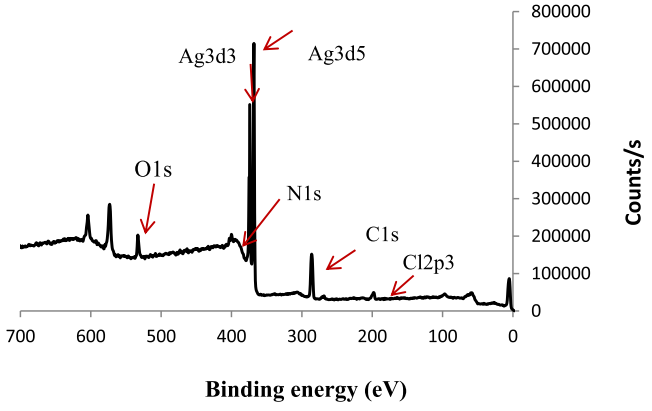

Figure 6. XPS Spectrum of AgNP-immobilized AEMs.

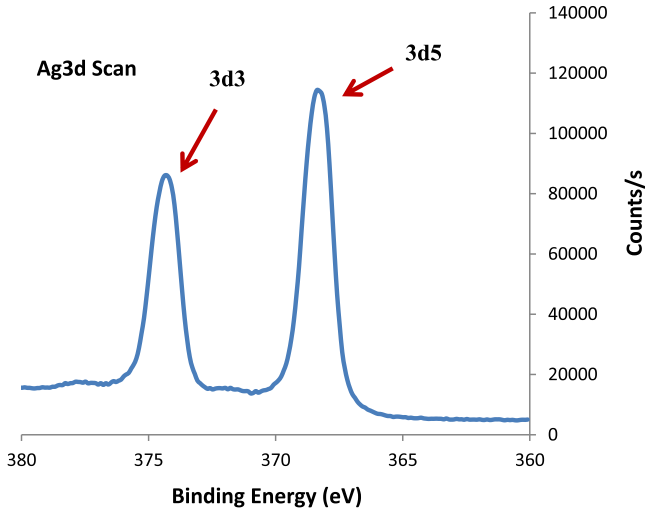

Figure 7. XPS spectrum of elements in the membrane structure.

https://doi.org/10.1021/acssuschemeng.3c06320
ACS Sustainable Chem. Eng. 2024, 12, 3977−3986

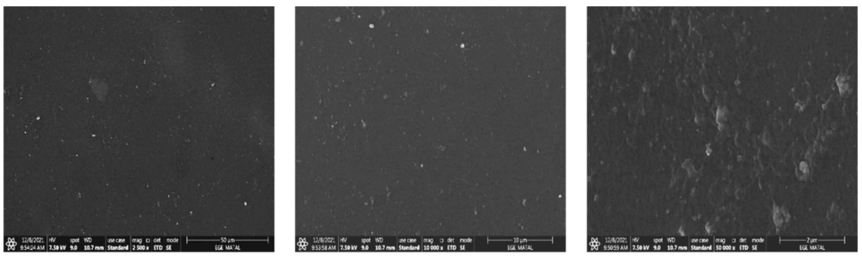

a b c

Figure 8. SEM surface images of the ER4-BR1.07 membrane before stability tests with the magnification of (a) 2500×, (b) 10,000×, and (c) 50,000×.

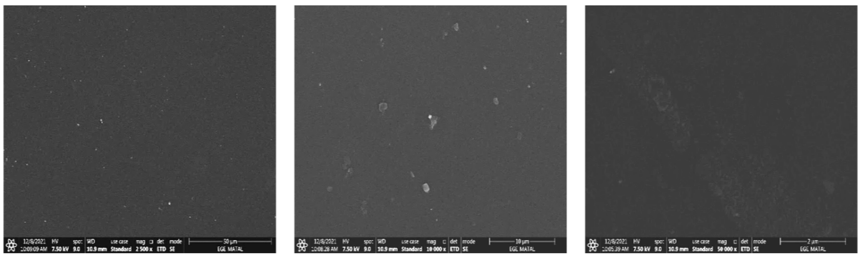

a b c

Figure 9. SEM surface images of the ER4-BR1.07 membrane after stability test in 0.017 M NaCl at 1 h with the magnification of (a) 2500×, (b) 10,000×, and (c) 50,000×.

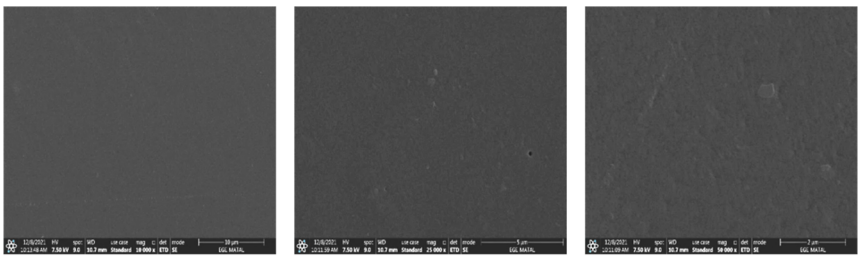

a b c

Figure 10. SEM surface images of the ER4-BR1.07 membrane after stability test in 0.017 M NaCl at 6 h with the magnification of (a) 2500×, (b) 25,000×, and (c) 50,000×.

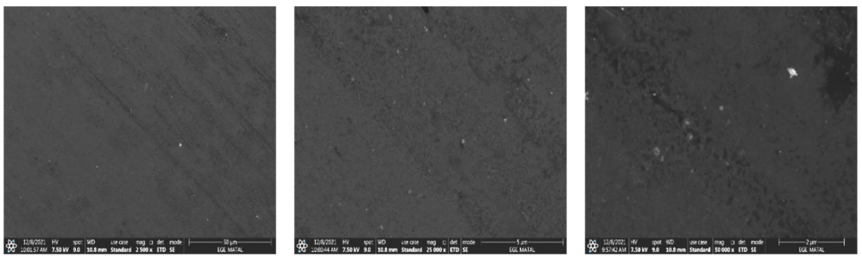

a b c

Figure 11. SEM surface images of the ER4-BR1.07 membrane after stability test in 0.5 M NaCl at 1 h with the magnification of (a) 2500×, (b) 25,000×, and (c) 50,000×.

3.2. Stability Test of AgNP-Immobilized AEMs.

Stability tests were carried out to see and determine the release of AgNPs from the AgNP-immobilized AEMs when the AEMs are in contact with NaCl solutions at different concentrations and time. If the amount of AgNPs released is high, the resistance of AEMs to biofouling will decrease. It is aimed to keep the AgNP release from AEMs as low as possible. The SEM images depicted in Figure 8 show the distribution of AgNPs on the membrane surface. The SEM images of the AgNP-immobilized AEMs after contact with 0.017 and 0.5 M NaCl solutions for different periods are shown in Figures 9−12.

It was considered that the amount of AgNPs on the AEM seemed to decrease to some extent after contact with NaCl solutions (Figures 9−12). However, there was no clear information from SEM images. Some information about release of AgNPs from the membrane surface is obtained from XPS analyses as well. The XPS analyses were carried out to see the atomic percentages of the AgNP-immobilized AEMs before and after exposure to NaCl solutions. The percentages

https://doi.org/10.1021/acssuschemeng.3c06320
ACS Sustainable Chem. Eng. 2024, 12, 3977−3986

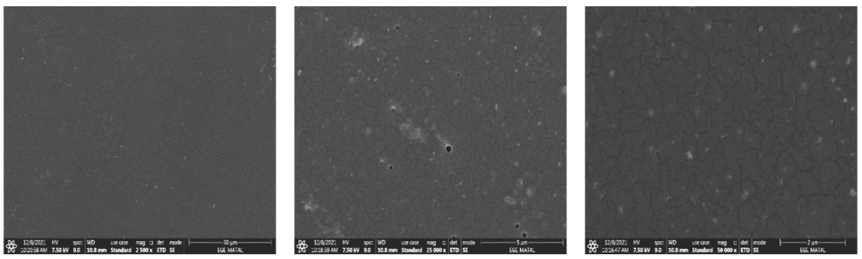

Figure 12. SEM surface images of the ER4-BR1.07 membrane after stability test in 0.5 M NaCl at 6 h with the magnification of (a) 2500×, (b) 25,000×, and (c) 50,000×.

of elements on the membrane surface-immobilized AgNPs before and after the stability test are given in Table 5. The

Table 5. Percentage of Elements in AgNPs Immobilized by AEMs by XPS Analysis

contact condition with NaCl solution	S (%)	C (%)	Cl (%)	Ag (%)	N (%)	O (%)
no contact	0.32	82.62	0.47	0.15	4.18	11.82
0.017 M NaCl-1 h	0.18	67.83	1.92	0.17	9.14	20.76
0.017 M NaCl-6 h	0.77	72.68	2.91	0.18	8.83	14.63
0.5 M NaCl-1 h	0.23	74.20	2.82	0.06	7.83	14.86
0.5 M NaCl-6 h	0.85	74.60	2.16	0.05	8.98	13.37

amount of AgNPs on the membrane surface decreased by contacting the membrane with especially 0.5 M NaCl solution. However, approximately the same atomic percentage values were obtained after 1 and 6 h of contacts with 0.017 M NaCl solution.

In addition, the ICP−MS measurements were carried out to observe the AgNP leakage from the membrane and to determine the amount of AgNPs immobilized on the AEMs before and after the contact in NaCl solutions. The amount of Ag on the AEMs can be seen in Table 6. A maximum amount

Table 6. Amount of AgNPs Immobilized on the AEMs

condition	Ag (μg/L) remained on the membrane
no contact with NaCl	185 ± 9 (loading amount)
0.017 M NaCl-1 h	74 ± 5
0.017 M NaCl-6 h	42 ± 3
0.5 M NaCl-1 h	11.2 ± 0.8
0.5 M NaCl-6 h	16.8 ± 0.8

of Ag was observed for the membrane which is not in contact with NaCl solution. The amount of Ag decreased with an increasing NaCl concentration in the contact solution.

3.3. Antibacterial Activity of AEMs. Figure 13 shows the antibacterial test results obtained with unmodified AEMs and AgNP-immobilized AEMs. Figure 13a shows the results of the control group which is the incubated medium without membrane, while Figure 13b,c shows the results of the AEMs and AgNP-immobilized AEMs. Figure 14 indicates the quantification of bacterial viability. The results show that the bacterial viability was dramatically decreased after immobilization of AgNPs to the membrane surface. The unmodified AEMs had a 1 log reduction (antibacterial rate, 90%) observed in the viability of the bacteria, while a 5.5 log reduction (antibacterial rate, 99.999%) was observed in the case of AgNP-immobilized AEMs. Similarly, in the study of Zhu et al.,

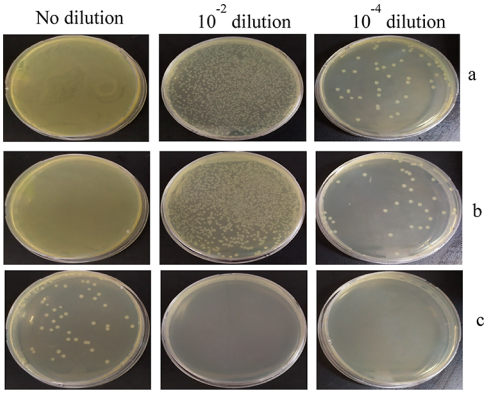

Figure 13. Results of the antibacterial tests. (a) Control (incubated medium without membrane), (b) unmodified AEMs, and (c) AgNP-immobilized AEMs.

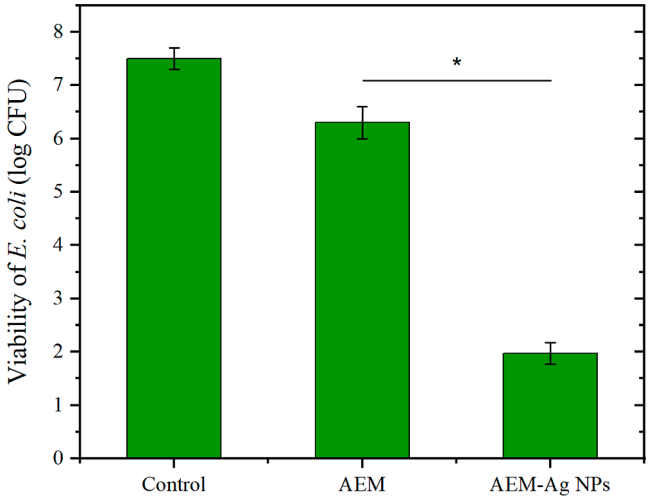

Figure 14. Antibacterial activity of the unmodified and AgNP-immobilized AEMs against *E. coli* (control; incubated medium without membrane) (* donates $p \leq 0.05$ significance between membranes).

AgNPs were immobilized onto the surface of a chitosan membrane to examine the antibiofouling performance of the membrane surface, and bare membrane had a significantly higher bacterial coverage than the silver-immobilized membranes.[29] Li et al. pointed to the possibility that AgNPs may alter the structure of bacterial cell membranes and reduce the activity of certain membranous enzymes, ultimately leading to the death of *E. coli* bacteria.[30] In the study of Vaselbehagh et al., the results demonstrated that AEM's antibiofouling characteristics were enhanced by a polydopamine layer during

https://doi.org/10.1021/acssuschemeng.3c06320
ACS Sustainable Chem. Eng. 2024, 12, 3977−3986

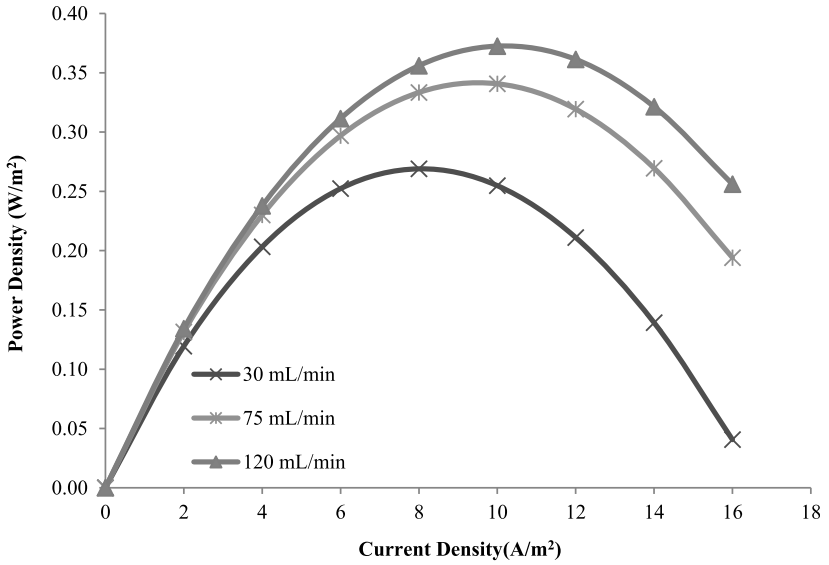

Figure 15. Power density vs current density graph of short-term studies of AgNP-immobilized PECH-C membranes coupled with NEOSEPTA CMX.

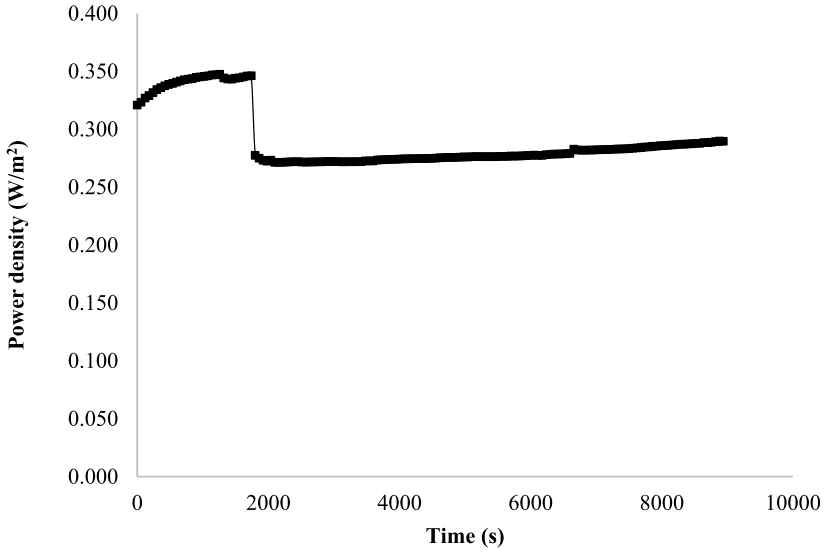

Figure 16. Power density vs time plot for long-term studies of AgNP-immobilized PECH-C coupled with NEOSEPTA CMX.

Table 7. Short-Term Studies of Unmodified and AgNP-Immobilized AEMs Coupled with NEOSEPTA CMX

membranes	salt ratio (g NaCl/L: g NaCl/L)	number of membrane pairs	flow rate of feed solutions (mL/min)	maximum power density (W/m^2)	open-circuit voltage (V)
AgNP-immobilized AEMs and NEOSEPTA CMX	1:30	3	30	0.269	0.409
			75	0.341	0.442
			120	0.372	0.448
AEMs and NEOSEPTA CMX			30	0.316	0.424
			60	0.275	0.433
			90	0.269	0.433
			120	0.264	0.433

RED operation.[17] Sile-Yuksel et al. showed that the best antibacterial effects were seen in nanocomposite membranes that incorporated surface AgNP storage.[31] In the study of Radzig et al., it has been observed that AgNPs can inhibit the growth of Gram-negative bacteria in both planktonic cells and biofilms.[18]

3.4. RED Test Results. Karakoç and Güler found that the highest power density produced by PECH-C (ER2-BR0.6)-type membranes coupled with NEOSEPTA CMX was 0.32 W/m^2, and it was 0.39 W/m^2 for NEOSEPTA AMX and NEOSEPTA CMX.[32] In this study, AgNP-immobilized ER2-BR0.6 membranes were used as AEMs, and NEOSEPTA CMX membranes were used as CEMs. At the same time, the effect of

https://doi.org/10.1021/acssuschemeng.3c06320
ACS Sustainable Chem. Eng. 2024, 12, 3977−3986

feed flow rate was investigated. In the RED test, the flow rate of electrode solution was adjusted as 300 mL/min, while flow rates of feed solutions were 30, 75, and 120 mL/min. The salt ratio was 1:30 (g NaCl/L less-saline solution/g NaCl/L high-saline solution), and the number of membrane pairs was 3.

The power density vs current density graphs obtained at different feed flow rates are depicted in Figure 15. The power density values increased with increasing flow rate and reached their highest value with 0.372 W/m^2.

The power density vs time plot of AgNP-immobilized PECH-C coupled with NEOSEPTA CMX during a long-term study is shown in Figure 16. The highest power density value obtained was 0.348 W/m^2 during a long-term study.

The results obtained with short- and long-term RED studies are summarized in Tables 7 and 8. For PECH-C based AEMs paired with NEOSEPTA CMX and PECH-C membranes immobilized with AgNPs, the maximum power density values are 0.316 W/m^2 with 30 mL/min of feed flow rate and 0.372 W/m^2 with 120 mL/min of feed flow rate. For the AgNP-immobilized PECH-C AEMs, the open-circuit voltage values increased with an increasing flow rate. On the other hand, with PECH-C-based AEMs, the open-circuit voltage values decreased with increasing flow rate and fixed after 60 mL/min of feed flow rate. At 120 mL/min feed flow rate, the maximum power density value is higher with AgNP-immobilized PECH-C membranes. During long-term RED studies, maximum power densities of 0.222 and 0.348 W/m^2 were obtained for PECH-C membranes coupled with NEOSEPTA CMX and PECH-C membranes immobilized with AgNPs, respectively. The highest power density is obtained as 0.348 W/m^2 during long-term studies at 30 mL/min flow rate if we compare long-term and short-term studies. The maximum power density values increased due to the increase in conductivity in the AgNP-immobilized membranes.

Table 8. Long-Term Studies of Unmodified and AgNP-Immobilized AEMs Coupled with NEOSEPTA CMX

membranes	salt ratio (g NaCl/L: g NaCl/L)	number of membrane pairs	linear flow velocity of feed solutions (mL/min)	maximum power density (W/m^2)
AEMs and NEOSEPTA CMX	1	3	30	0.222
AgNP-immobilized AEMs and NEOSEPTA CMX				0.348

4. CONCLUSIONS

Novel AgNP-immobilized PECH-based AEMs were developed for the first time, demonstrating their potential in harnessing sustainable salinity gradient energy through the clean process of RED. It was observed that the particle distribution is homogeneous after the immobilization of the AgNPs produced at pH 6.0, and agglomerations were formed at pH 9.0. Although the percentages of AgNPs released from AEMs were high according to chemical analysis by ICP−MS, their antibacterial activity was still sufficient. The XPS results showed that AgNPs were immobilized uniformly on the membrane surface. A highest power density produced with AgNP-immobilized PECH-C membranes coupled with NEOSEPTA CMX was 0.348 W/m^2.

AUTHOR INFORMATION

Corresponding Authors

Enver Güler − *Department of Chemical Engineering, Atılım University, Ankara 06830, Türkiye;* orcid.org/0000-0001-9175-0920; Email: enver.guler@atilim.edu.tr

Nalan Kabay − *Department of Chemical Engineering, Ege University, İzmir 35100, Türkiye;* orcid.org/0000-0001-8516-6752; Email: nalan.kabay@ege.edu.tr

Authors

Mine Eti − *Department of Chemical Engineering, Ege University, İzmir 35100, Türkiye*

Aydın Cihanoğlu − *Department of Chemical Engineering, Ege University, İzmir 35100, Türkiye;* orcid.org/0000-0003-3401-2416

Kadriye Özlem Hamaloğlu − *Department of Chemical Engineering, Hacettepe University, Ankara 06800, Türkiye*

Esra Altıok − *Department of Chemical Engineering, Ege University, İzmir 35100, Türkiye*

Ali Tuncel − *Department of Chemical Engineering, Hacettepe University, Ankara 06800, Türkiye;* orcid.org/0000-0002-4341-1286

Complete contact information is available at: https://pubs.acs.org/10.1021/acssuschemeng.3c06320

Notes

The authors declare no competing financial interest.

ACKNOWLEDGMENTS

This study was supported through EIG Concert-Japan (project no. TÜBİTAK 118M804). Mine Eti acknowledges the scholarships given by TÜBİTAK. The authors acknowledge Mitsubishi Chemical, Japan, especially Ando Kiyoto, for getting PAN samples, ASTOM Co., Japan, for NEOSEPTA membranes and Osaka Soda Co., Japan, for PECH polymer. One of the authors, Aydın Cihanoğlu, would like to thank the financial support from TÜBİTAK through the National Postdoc project (project no. 118C549).

REFERENCES

(1) Post, J. W. Blue energy: Electricity production from salinity gradients by reverse electrodialysis. PhD Thesis, Wageningen University, 2009.

(2) Mikhaylin, S.; Bazinet, L. Fouling on ion-exchange membranes: classification, characterization and strategies of prevention and control. *Adv. Colloid Interface Sci.* **2016**, *229*, 34−56.

(3) Santoro, S.; Tufa, R. A.; Avcı, A. H.; Fontananova, E.; Di Profio, G.; Curcio, E. Fouling propensity in reverse electrodialysis operated with hypersaline brine. *Energy* **2021**, *228*, 120563.

(4) Rijnaarts, T.; Moreno, J.; Saakes, M.; de Vos, W.; Nijmeijer, K. Role of anion exchange membrane fouling in reverse electrodialysis using natural feed waters. *Colloids Surf., A* **2019**, *560*, 198−204.

(5) Vermaas, D. A.; Kunteng, D.; Saakes, M.; Nijmeijer, K. Fouling in reverse electrodialysis under natural conditions. *Water Res.* **2013**, *47*, 1289−1298.

(6) Kotoka, F.; Merino-Garcia, I.; Velizarov, S. Surface modifications of anion exchange membranes for an improved reverse electrodialysis process performance: A review. *Membranes* **2020**, *10*, 160.

(7) Alabi, A.; AlHajaj, A.; Cseri, L.; Szekely, G.; Budd, P.; Zou, L. Review of nanomaterials-assisted ion exchange membranes for electromembrane desalination. *npj Clean Water* **2018**, *1*, 10.

(8) Cuiming, W.; Tongwen, X.; Weihua, Y. Fundamental studies of a new hybrid (inorganic-organic) positively charged membrane: membrane preparation and characterizations. *J. Membr. Sci.* **2003**, *216*, 269−278.

(9) Zhao, Y.; Tang, K.; Liu, H.; Van der Bruggen, B.; Sotto Díaz, A.; Shen, J.; Gao, C. An anion exchange membrane modified by alternate electro-deposition layers with enhanced monovalent selectivity. *J. Membr. Sci.* **2016**, *520*, 262−271.
(10) Ahmad, M.; Tang, C.; Yang, L.; Yaroshchuk, A.; Bruening, M. L. Layer-by-layer modification of aliphatic polyamide anion-exchange membranes to increase Cl^-/SO_4^{2-} selectivity. *J. Membr. Sci.* **2019**, *578*, 209−219.
(11) Rijnaarts, T.; Reurink, D. M.; Radmanesh, F.; de Vos, W. M.; Nijmeijer, K. Layer-by-layer coatings on ion exchange membranes: Effect of multilayer charge and hydration on monovalent ion selectivities. *J. Membr. Sci.* **2019**, *570*−*571*, 513−521.
(12) You, S. J.; Semblante, G. U.; Lu, S. C.; Damodar, R. A.; Wei, T. C. Evaluation of the antifouling and photocatalytic properties of poly(vinylidene fluoride) plasma-grafted poly(acrylic acid) membrane with self-assembled TiO_2. *J. Hard Mater.* **2012**, *237*−*238*, 10−19.
(13) Sprick, C. G. Functionalization of silver nanoparticles on membranes and its influence on biofouling. MSc. Thesis, University of Kentucky, 2017.
(14) Li, J.-H.; Shao, X.-S.; Zhou, Q.; Li, M.-Z.; Zhang, Q.-Q. The double effects of silver nanoparticles on the PVDF membrane: surface hydrophilicity and antifouling performance. *Appl. Surf. Sci.* **2013**, *265*, 663−670.
(15) Hao, L.; Liao, J.; Jiang, Y.; Zhu, J.; Li, J.; Zhao, Y.; Van der Bruggen, B.; Sotto, A.; Shen, J. Sandwich"-like structure modified anion exchange membrane with enhanced monovalent selectivity and fouling resistant. *J. Membr. Sci.* **2018**, *556*, 98−106.
(16) Jiang, S.; Wang, F.; Cao, X.; Slater, B.; Wang, R.; Sun, H.; Wang, H.; Shen, X.; Yao, Z. Novel application of ion exchange membranes for preparing effective silver and copper based antibacterial membranes. *Chemosphere* **2022**, *287*, 132131.
(17) Vaselbehagh, M.; Karkhanechi, H.; Takagi, R.; Matsuyama, H.; Matsuyama, H. Biofouling phenomena on anion exchange membranes under the reverse electrodialysis process. *J. Membr. Sci.* **2017**, *530*, 232−239.
(18) Radzig, M. A.; Nadtochenko, V. A.; Koksharova, O. A.; Kiwi, J.; Lipasova, V. A.; Khmel, I. A. Antibacterial effects of silver nanoparticles on gram-negative bacteria: Influence on the growth and biofilms formation, mechanisms of action. *Colloids Surf., B* **2013**, *102*, 300−306.
(19) Vaselbehagh, M.; Karkhanechi, H.; Mulyati, S.; Takagi, R.; Matsuyama, H. Improved antifouling of anion-exchange membrane by polydopamine coating in electrodialysis process. *Desalination* **2014**, *332*, 126−133.
(20) Gao, H.; Zhang, B.; Tong, X.; Chen, Y. Monovalent-anion selective and antifouling polyelectrolytes multilayer anion exchange membrane for reverse electrodialysis. *J. Membr. Sci.* **2018**, *567*, 68−75.
(21) Eti, M.; Cihanoğlu, A.; Güler, E.; Gomez-Coma, L.; Altıok, E.; Arda, M.; Ortiz, I.; Kabay, N. Further development of polyepichlorohydrin based anion exchange membranes for reverse electrodialysis by tuning cast solution properties. *Membranes* **2022**, *12*, 1192.
(22) Qin, Y.; Ji, X.; Jing, J.; Liu, H.; Wu, H.; Yang, W. Size control over spherical silver nanoparticles by ascorbic acid reduction. *Colloids Surf., A* **2010**, *372*, 172−176.
(23) Cihanoğlu, A.; Altınkaya, S. A facile route to the preparation of antibacterial polysulfone-sulfonated polyethersulfone ultrafiltration membranes using a cationic surfactant cetyltrimethylammonium bromide. *J. Membr. Sci.* **2020**, *594*, 117438.
(24) Steinigeweg, D.; Schlücker, S. Monodispersity and size control in the synthesis of 20−100 nm quasi-spherical silver nanoparticles by citrate and ascorbic acid reduction in glycerol-water mixtures. *Chem. Commun.* **2012**, *48*, 8682−8684.
(25) Agnihotri, S.; Mukherji, S.; Mukherji, S. Size-controlled silver nanoparticles synthesized over the range 5−100 nm using the same protocol and their antibacterial efficacy. *RSC Adv.* **2014**, *4*, 3974−3983.
(26) Mikac, L.; Ivanda, M.; Gotic, M.; Mihelj, T.; Horvat, L. Synthesis and characterization of silver colloidal nanoparticles with different coatings for SERS application. *J. Nanopart. Res.* **2014**, *16*, 2748.
(27) Kamali, M.; Ghorashi, A. A. S.; Asadollahi, M. A. Controllable synthesis of silver nanoparticles using citrate as complexing agent: characterization of nanoparticles and effect of pH on size and crystallinity. *Iran. J. Chem. Chem. Eng.* **2012**, *31* (4), 221−228.
(28) Rashid, M. U.; Bhuiyan, K. H.; Quayum, M. E. Synthesis of silver nano particles (Ag-NPs) and their uses for quantitative analysis of vitamin C tablets. *Dhaka Univ. J. Pharm. Sci.* **2013**, *12* (1), 29−33.
(29) Zhu, X.; Bai, R.; Wee, K. H.; Liu, C.; Tang, S. L. Membrane surfaces immobilized with ionic or reduced silver and their anti-biofouling performances. *J. Membr. Sci.* **2010**, *363*, 278−286.
(30) Li, W.; Xie, X.; Shi, Q.; Zeng, H.; Ou-Yang, Y. S.; Chen, Y. Antibacterial activity and mechanism of silver nanoparticles on *Escherichia coli*. *Appl. Microbiol. Biotechnol.* **2010**, *85*, 1115−1122.
(31) Sile-Yuksel, M.; Tas, B.; Koseoglu-Imer, D. Y.; Koyuncu, I. Effect of silver nanoparticle (AgNP) location in nanocomposite membrane matrix fabricated with different polymer type on antibacterial mechanism. *Desalination* **2014**, *347*, 120−130.
(32) Karakoç, E.; Güler, E. Comparison of physicochemical properties of two types of polyepichlorohydrin-based anion exchange membranes for reverse electrodialysis. *Membranes* **2022**, *12*, 257.

https://doi.org/10.1021/acssuschemeng.3c06320
ACS Sustainable Chem. Eng. 2024, 12, 3977−3986